Electronic Supplementary Material (ESI) for Journal of Materials Chemistry A.

Tunable Built-in Electric Fields Enable High-performance One-Dimensional Co-axial MoO_x/MoON Heterojunction Nanotube Arrays for Thin-film Pseudocapacitive Charge Storage Devices

Bowen Jin,[a] Peng Chen,[b] Hongqi Chu,[a] Dan Zhang,[a] Shuangshuang Cui,[a] Xin Zhou,[a]* Min Yang [a]**

a MIIT Key Laboratory of Critical Materials Technology for New Energy Conversion and Storage, School of Chemistry and Chemical Engineering, Harbin Institute of Technology, Harbin 150001, China

b Key Laboratory of Functional Inorganic Material Chemistry (MOE), School of Chemistry and Materials Science, Heilongjiang University, Harbin, 150080, China

*Corresponding author E-mail:

jehugu@gmail.com (P.C), zhoux@hit.edu.cn (X.Z.), yangmin@hit.edu.cn (M.Y.)

XPS measurements

The Mo 3d spectrum of MoO_3 in Figure S9 exhibits the presence of two spin orbit split peaks at 236.2 and 233.05 eV, which are assigned to MoO_3[1]. In the case of the MoO_x, Mo^{6+}-O peaks in Mo 3d spectrum are shifted to a lower binding energy. And two new doublets located at 235.6/232.5 eV, 234.2/231.1 eV are appeared, which can be contributed to Mo^{6-x}-O (x<1) and Mo^{4+}-O, respectively [2,3]. For the MoON, a pair of new peaks located at 233.0/229.9 eV are appeared, relating to N-Mo-O. The O 1s spectrum of MoO_3 can be deconvoluted into two peaks located at 531.9 eV and 530.5 eV, corresponding to defect O and O-Mo species respectively (as shown in Figure S9). A binding energy of 529.8 eV confirmed the presence of Mo-O-N species in MoON after ammonification. The corresponding N 1s core level XPS spectrum of MoON is displayed to two peak regions located 395.5 and 397.2 eV are ascribed to Mo-N and Mo-N-O species [4,5].

Impedance simulation

Importantly, the H^+ intercalation process can be largely increased by BEF, which is beneficial to the capacitive performance. Electrochemical impedance spectroscopy (EIS) measurements were conducted to characterize the Warburg resistance of each nanotube arrays. Figure S15 shows an equivalent circuit based on EIS results, where R_s is the ohmic resistance; R_{ct} corresponds to charge transform resistance; Q represents to double layer capacitance with dispersion effect; W is Warburg resistance. Evidently, the Warburg resistance of MoO_x/MoON heterojunction nanotubes is largely decreased to 18.8 Ω comparing with that of MoO_x (10945 Ω) and MoON (87 Ω). This decrease can be ascribed to the BEF effects in heterojunction interface.

DFT calculation

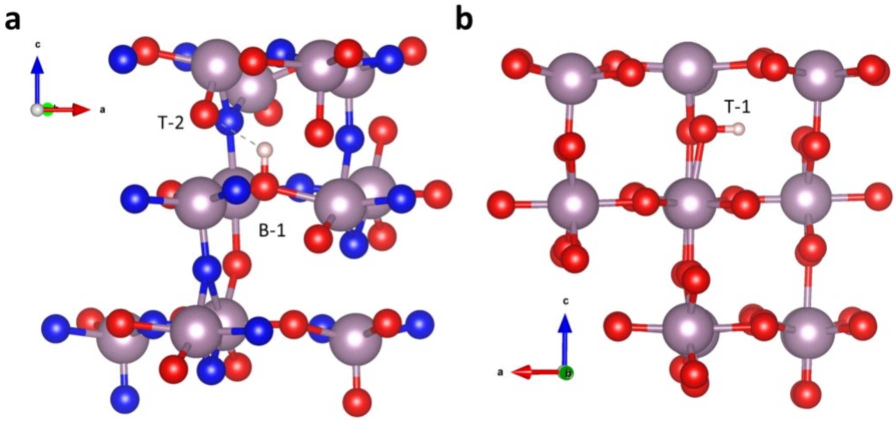

Figure S1 Optimized intercalation configuration for H^+ into MoON (a) and MoO_x (b).

Material characterization

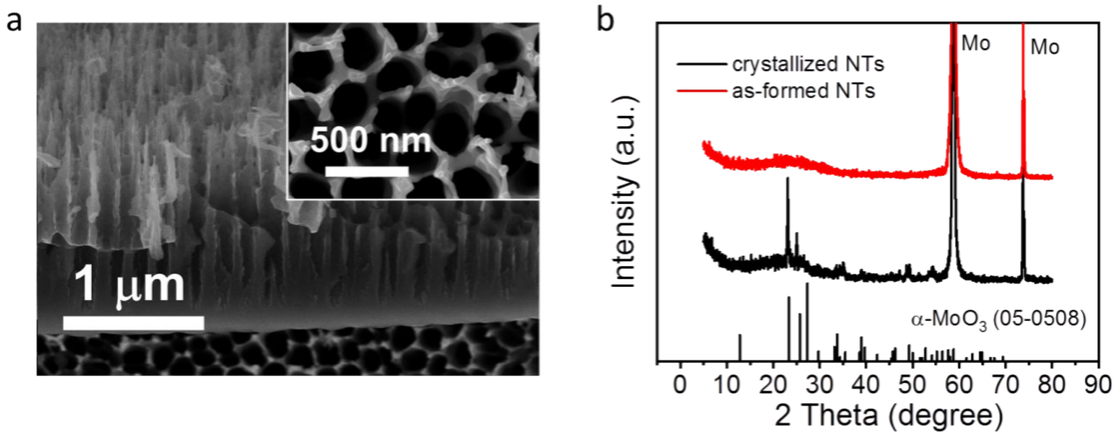

Figure S2 (a) SEM images of as-formed MoO_3 nanotubes; (b) XRD patterns of as-formed and crystallized MoO_3 nanotubes.

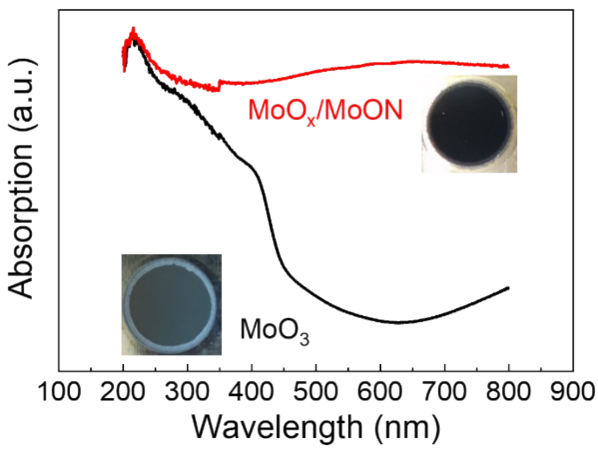

Figure S3 UV-Vis absorption spectra of MoO_3 and MoO_x/MoON nanotubes (inset: optical photos).

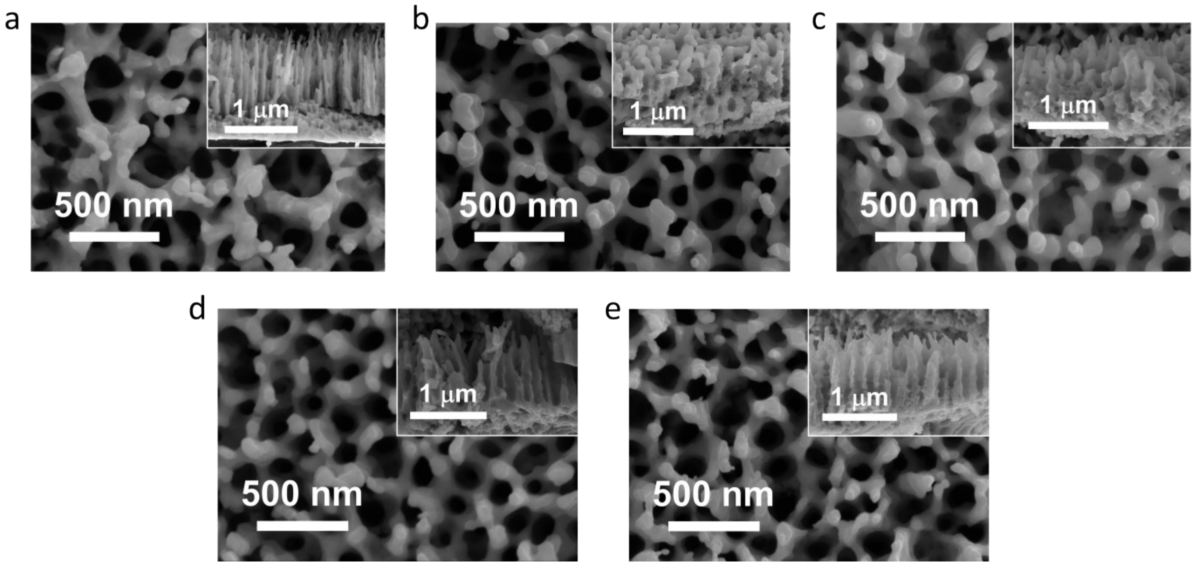

Figure S4 SEM images of MoO_3 nanotubes with ammonification for 2 h at (a) 300 ^{o}C; (b) 400 ^{o}C; (c) 450 ^{o}C and at 350 ^{o}C for 1 h (d) and 3 h (e).

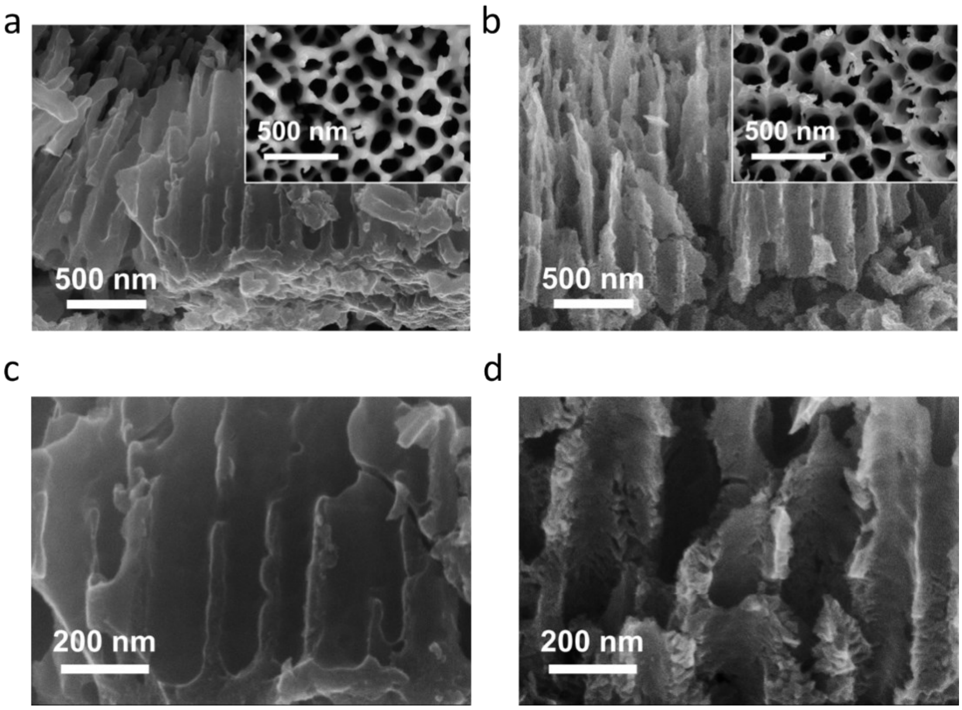

Figure S5 SEM images of (a) MoO_x nanotubes; (b) MoON nanotubes, and the tube walls of

MoO_x (c) and MoON nanotubes (d).

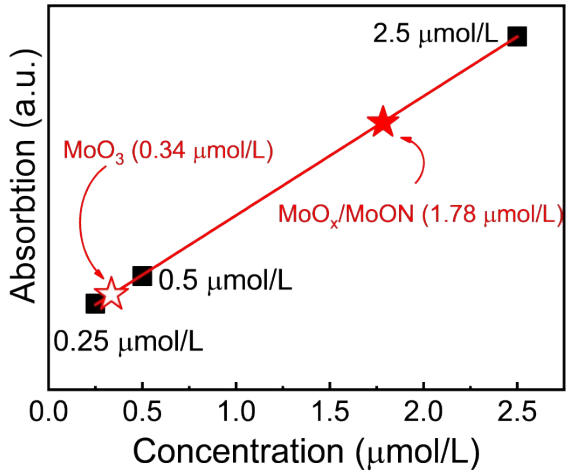

Figure S6 Dye absorption measurements of MoO_x nanotubes and MoO_x/MoON nanotubes.

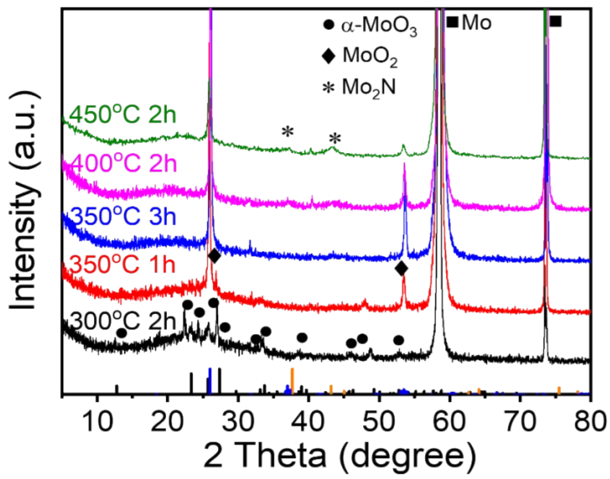

Figure S7 XRD patterns of MoO_3 nanotubes after ammonification at different temperatures and durations.

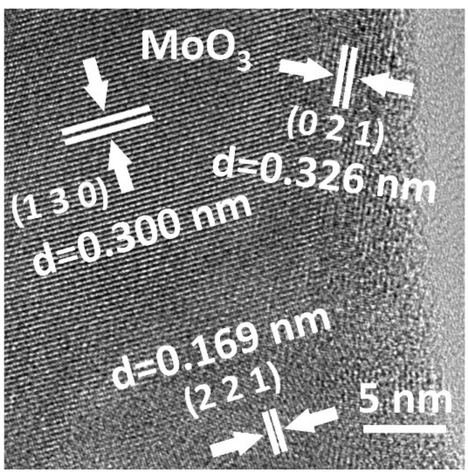

Figure S8 HRTEM image of α-MoO_3 nanotubes

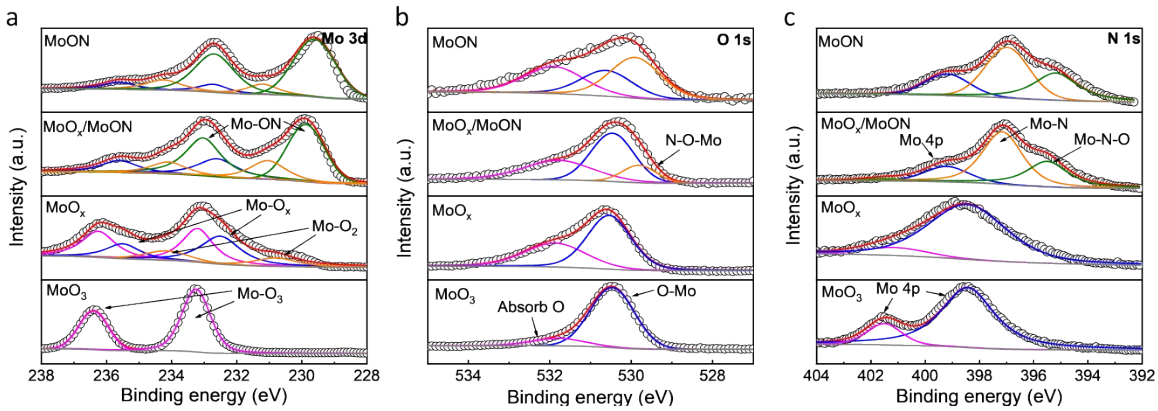

Figure S9 High resolution XPS spectra of MoO_3, MoO_x, MoO_x/MoON and MoON: (a) Mo 3d; (b) O 1s, and (c) N 1s.

Electrochemical measurements

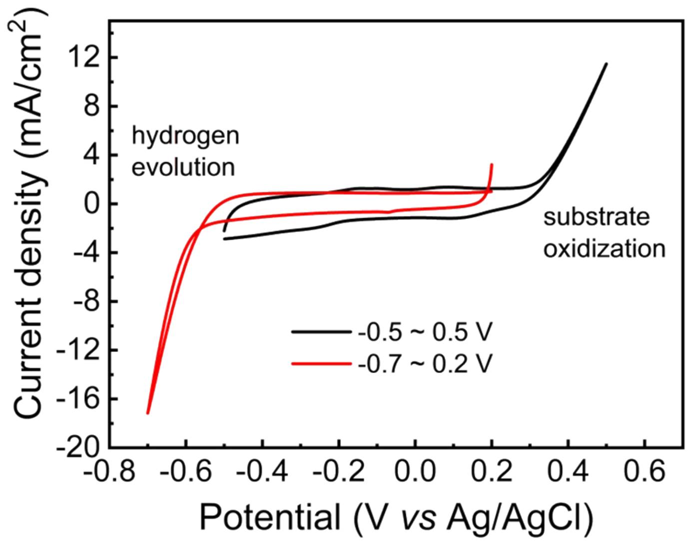

Figure S10 CV curves of MoO_x/MoON nanotubes with different potential ranges.

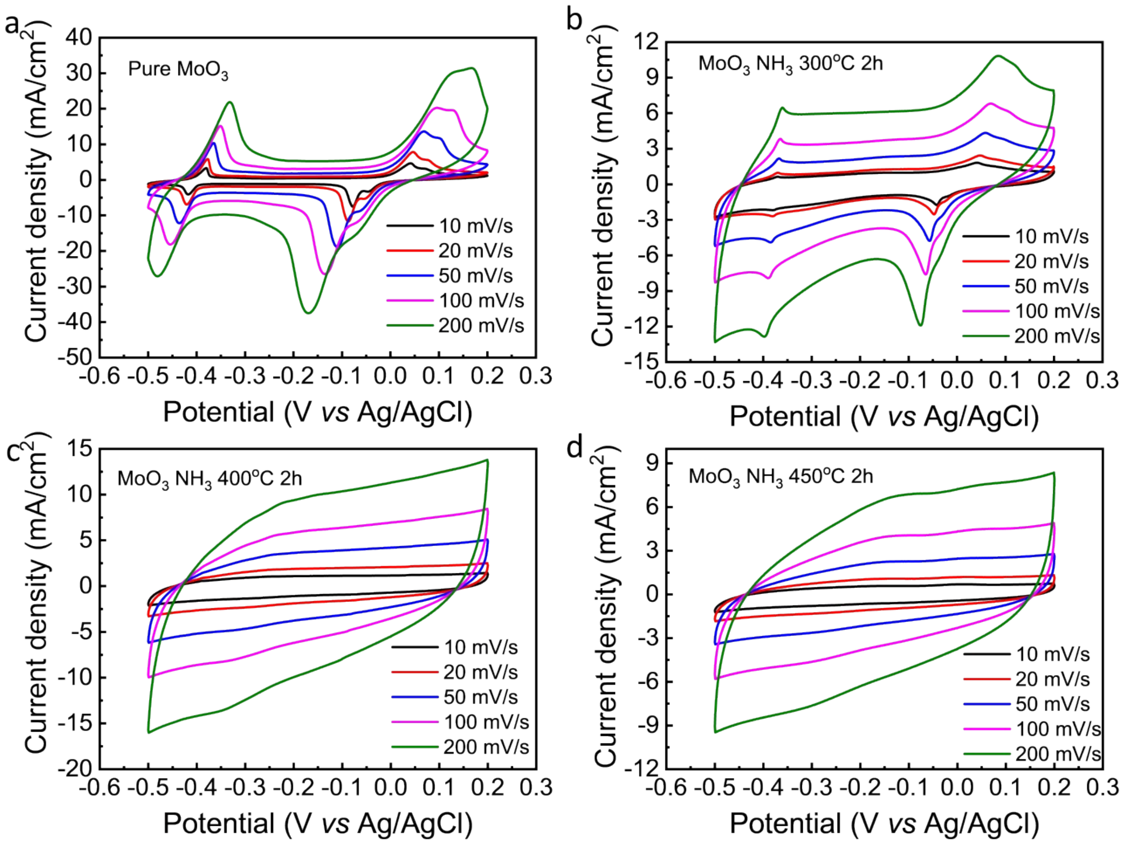

Figure S11 CV plots of MoO_3 nanotubes ammonificated at different temperatures for 2 h (a) crystallized MoO_3; (b) 300 °C; (c) 400 °C; (d) 450 °C.

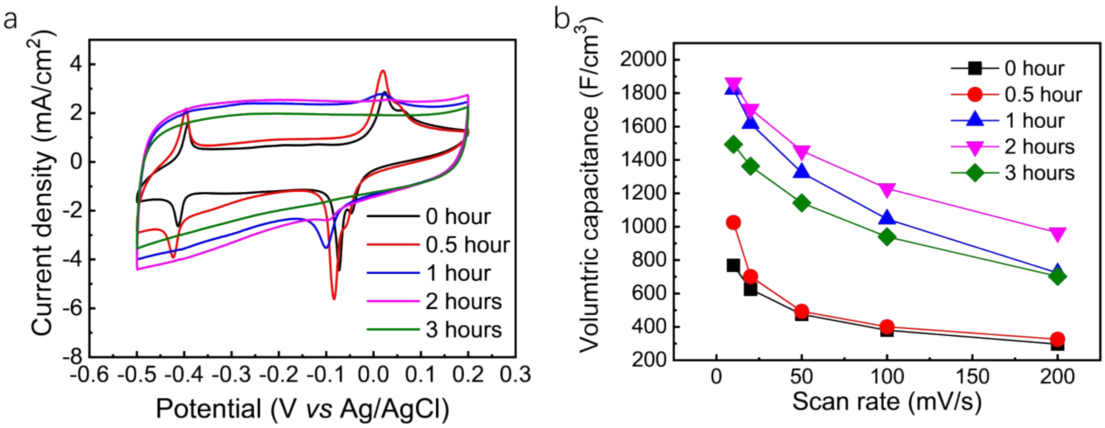

Figure S12 Electrochemical performance of MoO_3 nanotubes ammonificated at 350 °C for different time (a) CV plots and (b) volumetric capacitances.

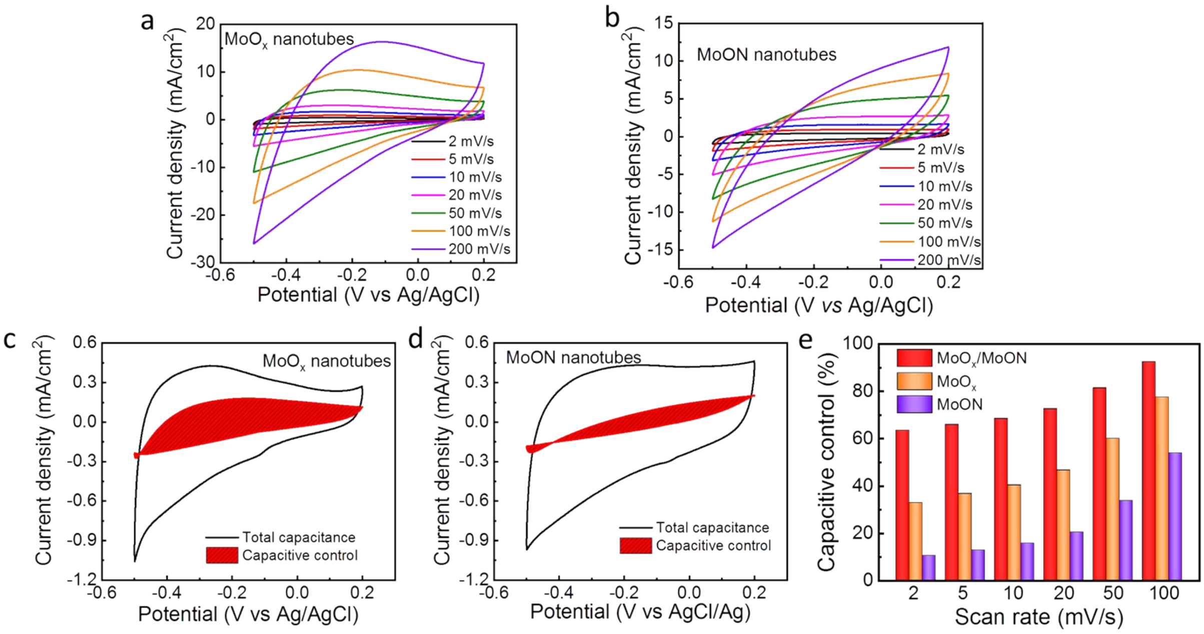

Figure S13 CV plots with different scan rates of MoO_x nanotubes (a) and MoON nanotubes (b); CV curve recorded with 2 mV/s of MoO_x (c) and MoON nanotubes (d) (shade curve is capacitive-controlled capacitance); (e) ratios of capacitive-controlled capacitance of MoO_x nanotubes and MoON nanotubes in total capacitance at different scan rates.

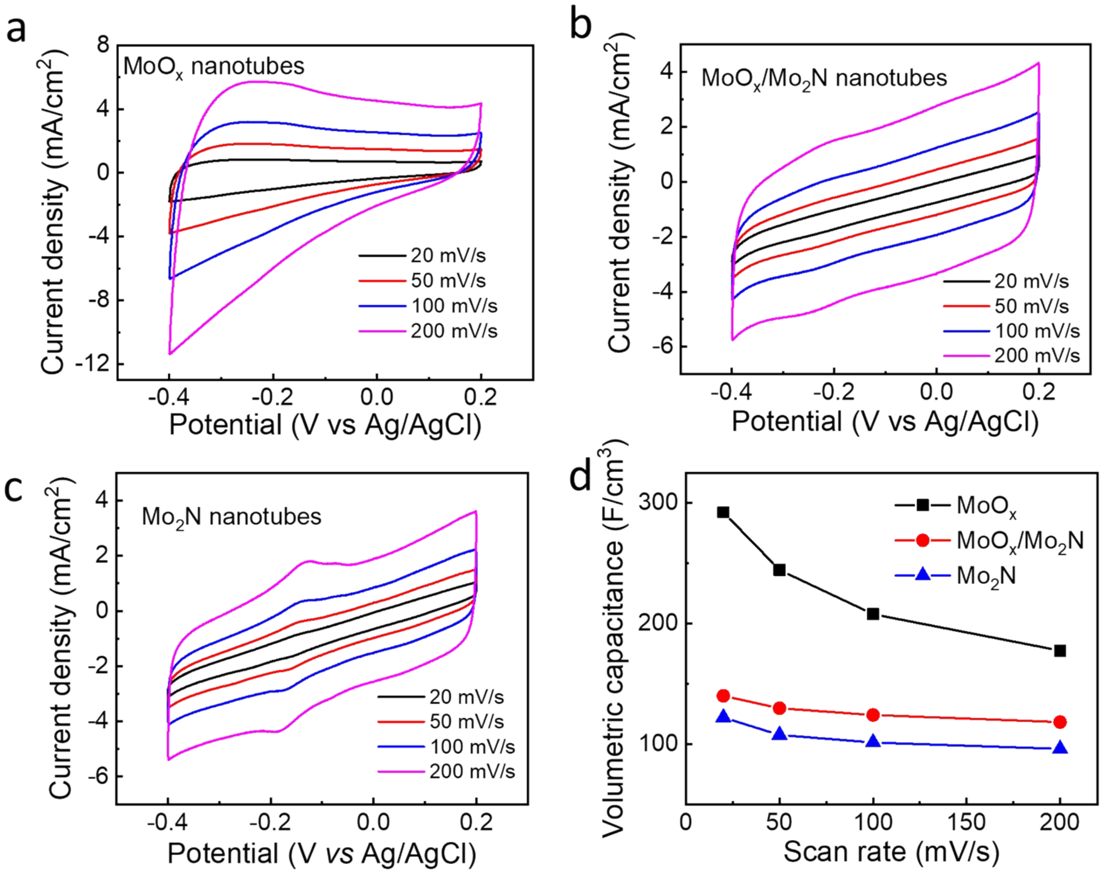

Figure S14 CV plots of (a)MoO$_x$ nanotubes; (b) MoO$_x$/Mo$_2$N nanotubes; (c) MoO$_x$ nanotubes; (d) relationships between scan rate and capacitance.

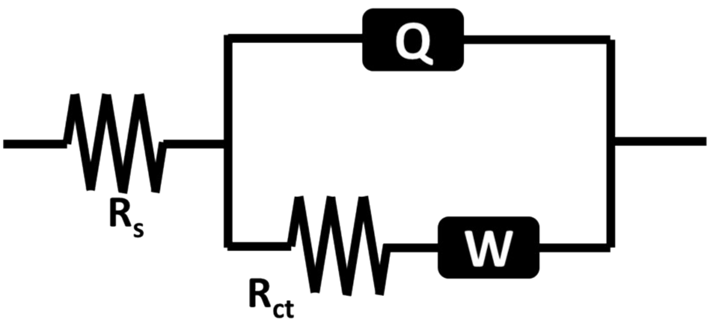

Figure S15 Randles equivalent circuit of EIS results in Fig.5f.

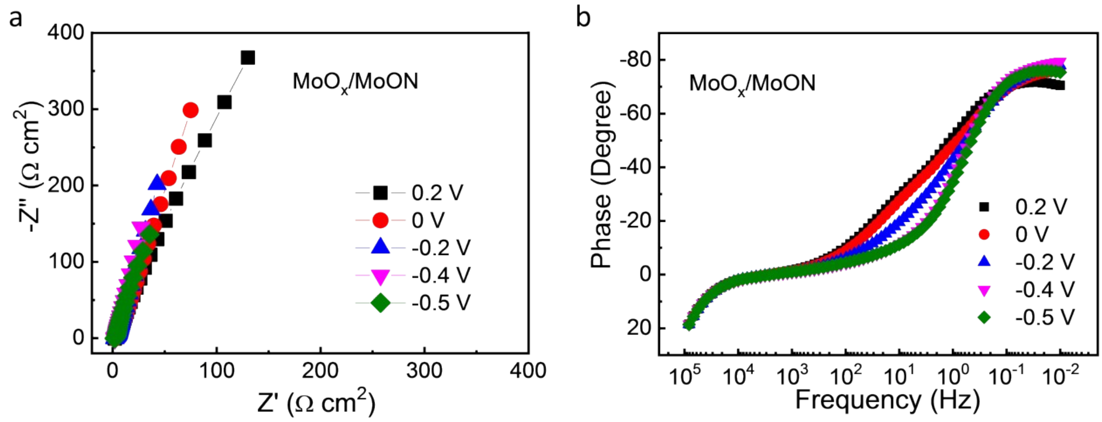

Figure S16 Nyquist plots (a) and corresponding Bode plots (b) of MoO_x/MoON electrode at different potentials.

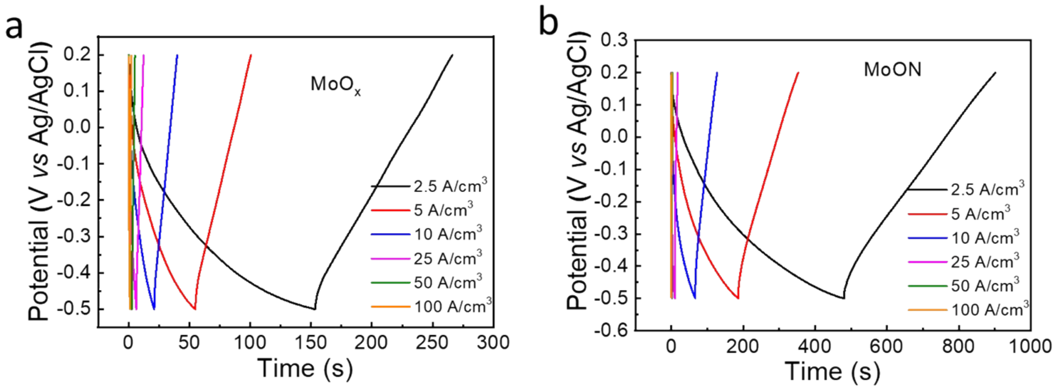

Figure S17 GCD plots of MoO_x nanotubes (a) and MoON nanotubes (b).

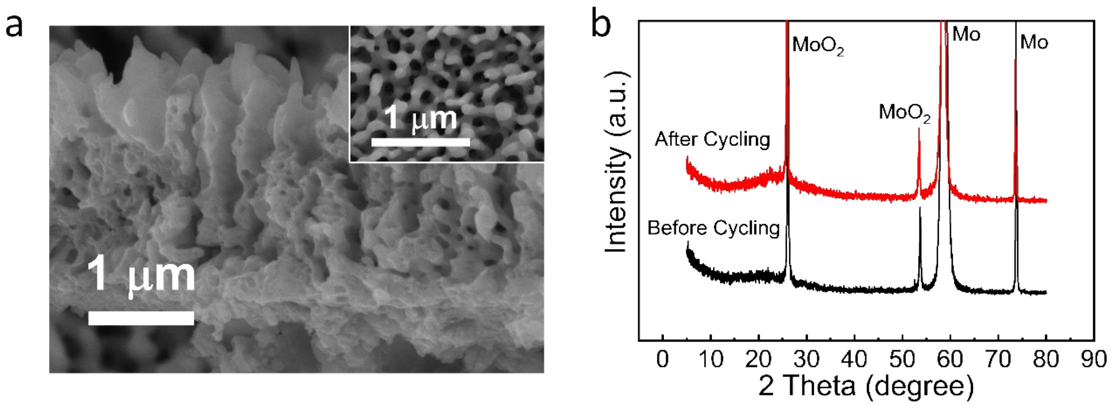

Figure S18 Morphology and crystal phase characterizations of MoO_x/MoON nanotubes after cycling (a) SEM images and (b) XRD patterns.

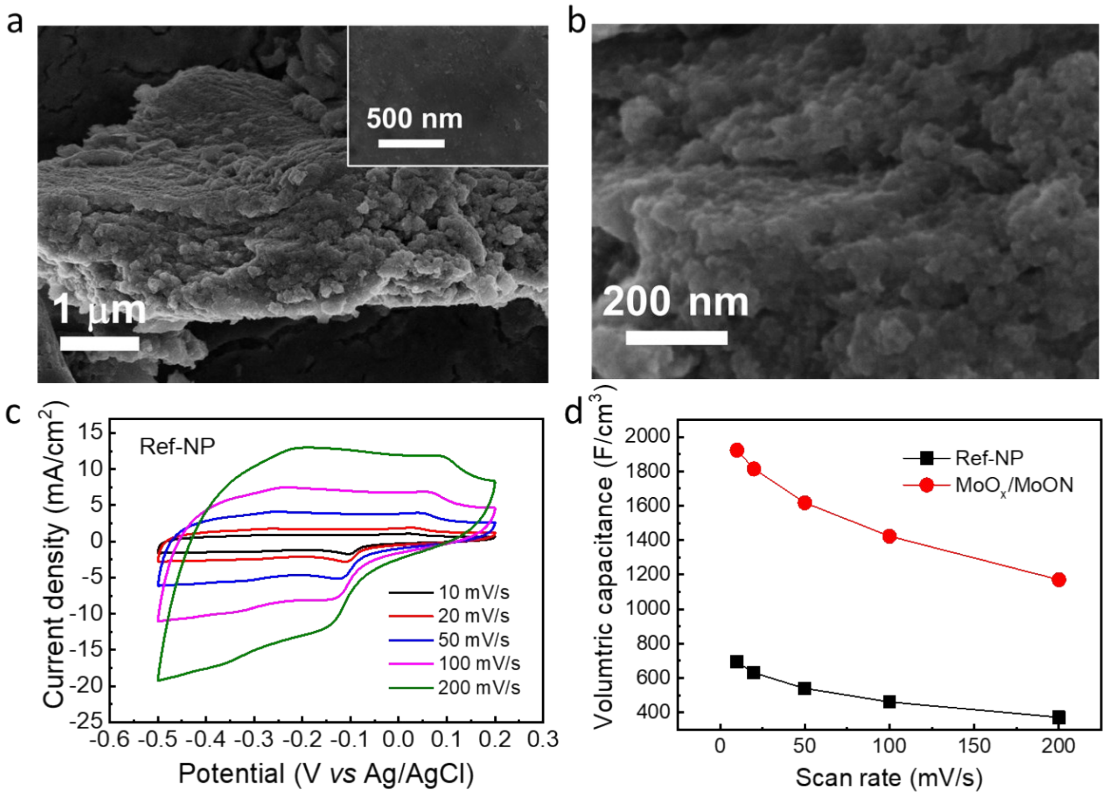

Figure S19 (a,b) SEM images of MoO_x/MoON nanoporous (Ref-NP); (c) CV plots of Ref-NP at different scan rates; (d) volumetric capacitance of MoO_x/MoON nanotubes and Ref-NP.

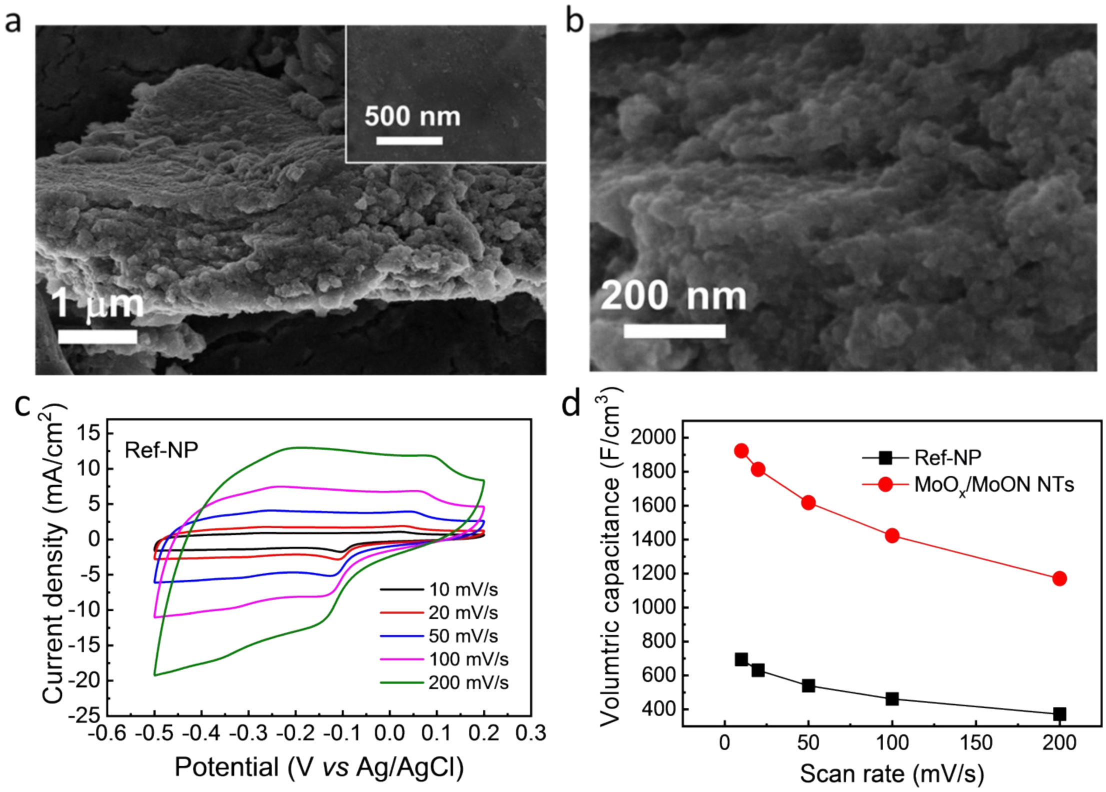

Figure S20 (a,b) SEM images of MoO_x/MoON nanotubes with 3 μm thickness; (c) CV plots of MoO_x/MoON with 3 μm thickness (d) volumetric capacitances of MoO_x/MoON nanotubes with different thicknesses.

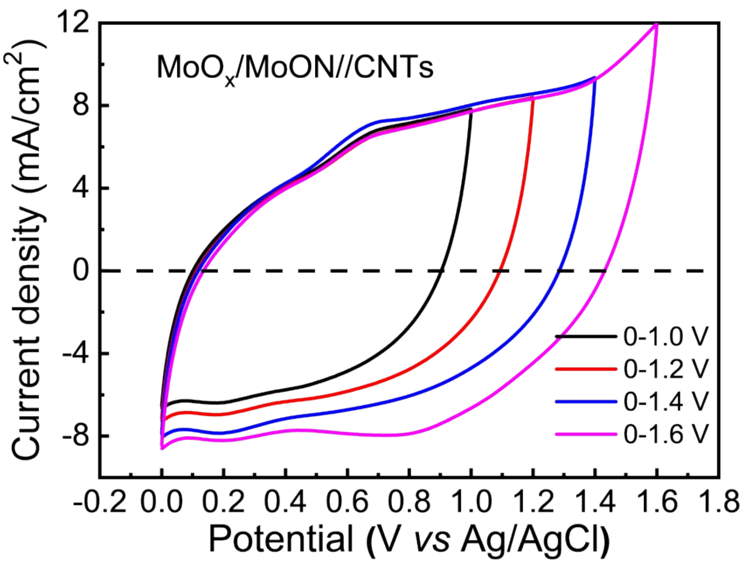

Figure S21 Asymmetric capacitor based MoO_x/MoON/CNTs in different voltage ranges.

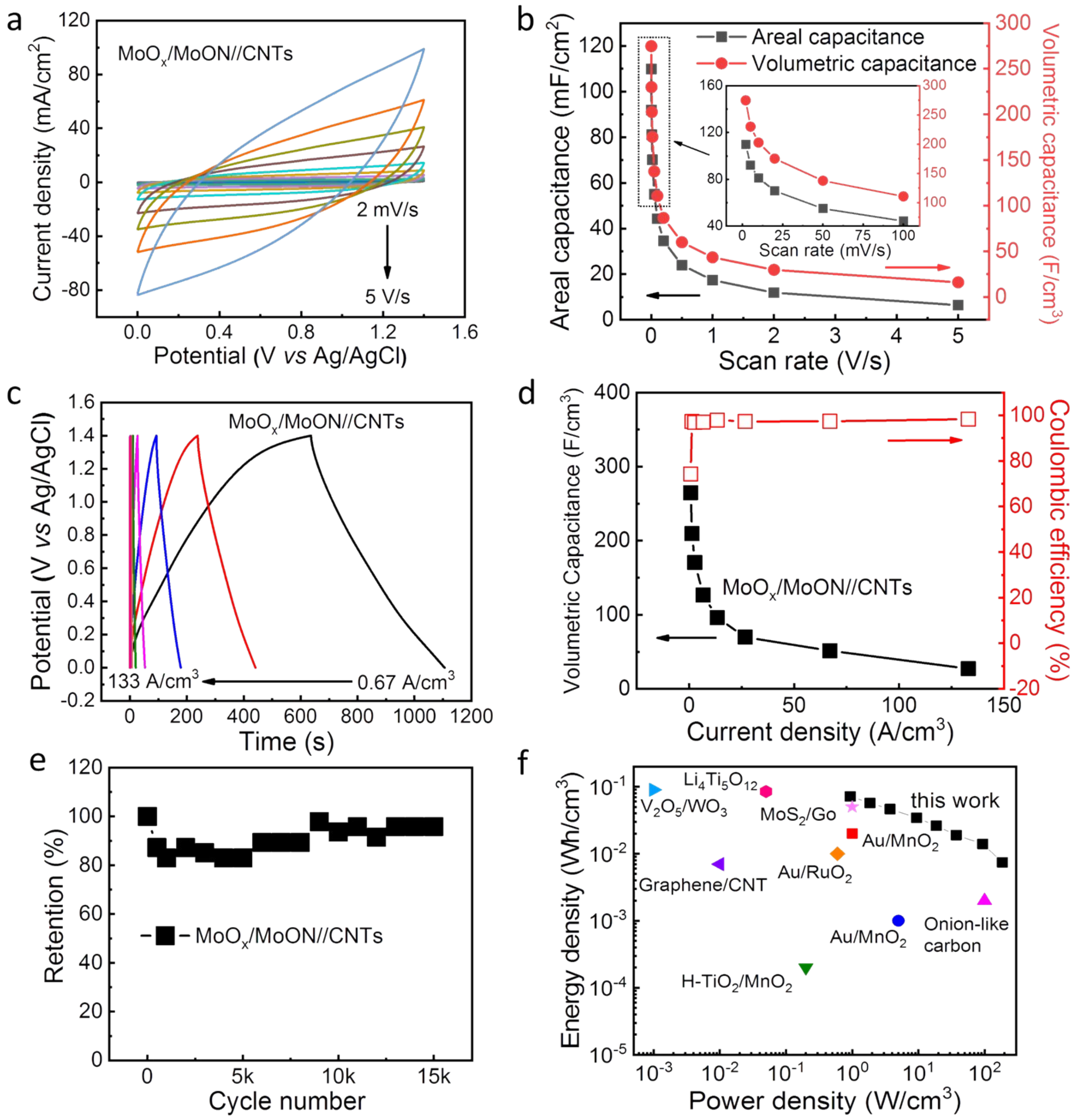

Figure S22 Electrochemical performances of asymmetric supercapacitor (a) CV plots at different scan rates; (b) areal capacitance and volumetric capacitance based on CV plots; (c) GCD plots at different charging rates; (d) volumetric capacitance at different charging rates based on GCD plots; (e) capacitance retention during cycling. (f) volumetric energy density of the ASC [6–8].

.

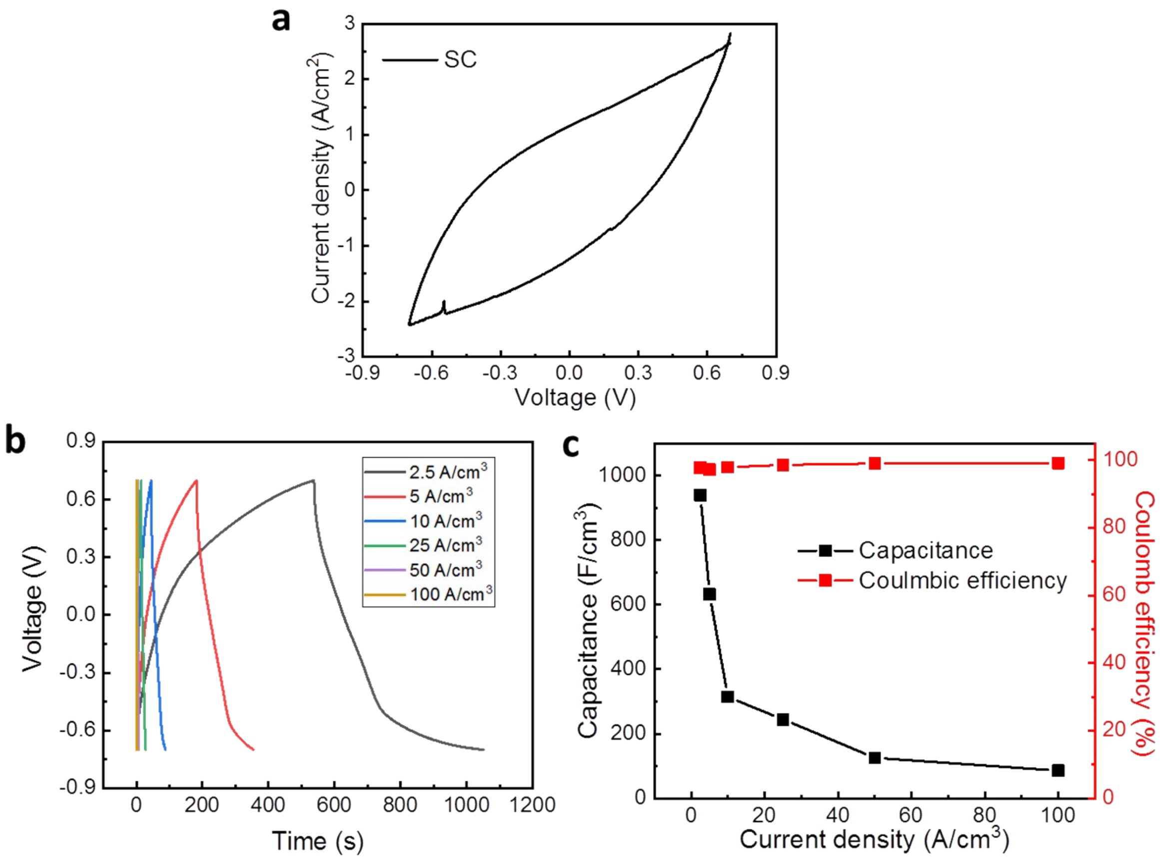

Fig. S23 Performance of SC device (a) the CV plot of SC device at 20 mV/s. (b) GCD plots of SC device at different current densities (c) Capacitance and Coulombic efficiency of SC device.

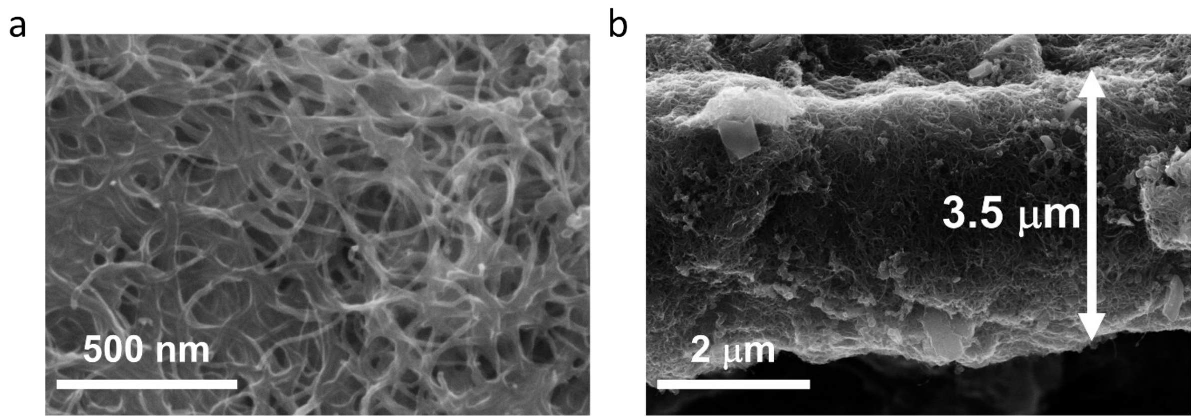

Figure S24 SEM images of CNTs electrode: (a) surface and (b) cross-section.

Table S1 The impedance fitting results of the MoO_x, MoON and MoO_x/MoON nanotubes in Figure 5f

		MoO_x	MoON	MoO_x/MoON
R_s (Ω)		2	1.45	2
R_{ct} (Ω)		1314	10	0.3
Warburg resistance (Ω)		10945	87	18.8
Q	**C (µF)**	0.002	0.03	0.02
	n	0.9	0.88	0.8

Table S2 Overview of most recent volumetric capacitances reported in the literature for various class of materials.

Material	Measurement condition	Volumetric Capacitance	Mass Capacitance	thickness	Method	Reference
MoO_x/MoON nanotubes	**2.5 A/cm^3 (1.1 A/g); 2 mV/s**	**1987 F/cm^3 2063 F/cm^3**	**883 F/g; 917 F/g**	**1.2 µm**	**Anodization**	**This work**
MoO_x/MoON nanotubes	**2 mV/s**	**1900 F/cm^3**		**3 µm**	**Anodization**	**This work**
Nanoporous Gold/MnO_2[9]	50 mV/s	1160 F/cm^3		100 nm	Electrodeposition	Nature Nanotechnology 2011, 6, 232
$Ti_3C_2T_x$[10]	1 A/g	350 F/cm^3	130 F/g (2 mV/s)	2 µm	Filtration	Science 2013, 341, 1502
$Ti_3C_2T_x$[11]	2 mV/s	900 F/cm^3	250 F/g	5 µm	Rolled	Nature 2014, 516, 78
MoS_2[12]	2 mV/s	650 F/cm^3		5 µm	Filtration	Nature Nanotechnology 2015, 10, 313

Graphene/Polyaniline[13]	0.5 A/g	800 F/cm^3	550 F/g		Hydrothemal and Press	Advanced Materials 2015, 27, 8082
Nanoporous NiCuMn Oxy-hydroxide[14]	0.25 A/cm^3	627 F/cm^3	1097 F/g	20 µm	electrodeposition	Angewandte Chemie-International Edition 2015, 54, 8100
Fe_2O_3@Fe_3O_4[15]	5 mV/s	1206 F/cm^3	231.9 F/g	1.2 µm	Hydrothemal	ACS Apply Materials Interfaces 2015, 7, 27518
Nitrogen doped graphene[16]	0.5 A/g	600 F/cm^3	500 F/g	26 µm	Paste	Advanced Energy Materials 2017, 7, 1700766
Compact graphene[17]	0.5 A/g	711 F/cm^3	450 F/g	5−6 µm	Hydrothemal and Press	Nano Letters 2017, 17, 1365
Graphene/PANI[18]	0.5 A/g	1058 F/cm^3	750 F/g	7 µm	Hydrothemal and Press	Journal of Materials Chemistry A 2017, 5, 16689
MXene/Graphene[19]	2 mV/s	1500 F/cm^3	375 F/g 3 µm 450 F/g 90 nm	3 µm	Filtration	Nature Energy 2017, 2, 10175
RuO_2/Graphene[20]	0.1 A/g	1485 F/cm^3	580 F/g		Hydrothemal and Press	Small 2017, 13,1701026
$NiCo_2O_4$@CNT/CNT[21]	0.5 A/g 2 mV/s	873 F/cm^3 795 F/cm^3	1177 F/g	24.3 µm	Filtration	Advanced Functional Materials 2017, 27, 1702160
Co_3O_4 Nanosheets[22]	12 A/cm^3	376 F/cm^3	-	1 µm	electrodeposition	Journal of Materials Chemistry A 2018, 6, 36
$Mo_{1.33}C$ Mxene /PEDOT:PSS[23]	2 mV/s	1310 F/cm^3	-	3 µm	Filtration	Advanced Functional Materials 2018, 28, 1703808
Graphene/MoS_2[24]	1 A/g 0.5 A/cm^3	1431 F/cm^3	707 F/g	20 µm	Filtration	Advanced Energy Materials 2018, 8, 1800227
2D mixed MXenes[25]	2 mV/s	1514 F/cm^3	435 F/g	0.18-3 µm	Filtration	ACS Apply Materials Interfaces 2018, 10, 25949
MXene/PANI[26]	2 mV/s	1682 F/cm^3	503 F/g	4 µm	Filtration	Journal of Materials Chemstry A, 2018, 6, 22123
NP c-V_2O_3/r-VO_{2-x}[8]	5 mV/s 1 A/g	1933 F/cm^3 1353 F/cm^3	1856 F/g	1.2 µm	-	Nature Communications 2018, 9, 1375

NP c-V_2O_3/r-VO_{2-x}[8]	2 mV/s	~1750 F/cm^3	~1700 F/g	7.8 μm	-	Nature Communications 2018, 9, 1375
Na-V_2CT_x[27]	5 mV/s	1315 F/cm^3	-	3~4 μm	Filtration	Advanced Materials 2019, 31, 1806931
AC/CNT/rGO[28]	5 mV/s	41.3 F/cm^3	186 F/g	5 μm	3D-printing	Advanced Energy Materials 2019, 9, 1802578
Carbon[29]	1 A/g	215 F/cm^3	235 F/g			Advanced Functional Materials 2019, 29, 1901127.
CeO_{2-x}[30]	5 mV/s	1873 F/cm^3		20 nm	Electrodeposition	Nature Communications 2019, 10, 2594
wavy MXene[31]	10 mV/s	1293 F/cm^3	340 F/g	6 μm	Filtration	Nano Energy 2020, 75, 104971
$Ti_3C_2T_x$/ rGO[32]	2 mV/s	1443 F/cm^3	-	-	co-assembly	Angewante Chemie International. Edition 2020, 59, 20628-20635

References

1 M. R. Smith and U. S. Ozkan, *J. Catal.*, 1993, 141, 124–139.

2 M. Anwar, C. A. Hogarth and R. Bulpett, *J. Mater. Sci.*, 1989, **24**, 3087–3090.

3 B. Brox and I. Olefjord, *Surf. Interface Anal.*, 1988, **13**, 3–6.

4 S. Wang, L. Li, Y. Shao, L. Zhang, Y. Li, Y. Wu and X. Hao, *Adv. Mater.*, 2019, **31**, 1806088.

5 K. Sharma, D. Hui, N. H. Kim and J. H. Lee, *Nanoscale*, 2019, **11**, 1205–1216.

6 G. Yilmaz, C. X. Guo and X. Lu, *ChemElectroChem*, 2016, **3**, 158–164.

7 F. Wang, Y. Li, Z. Cheng, K. Xu, X. Zhan, Z. Wang and J. He, *Phys. Chem. Chem. Phys.*, 2014, **16**, 12214.

8 B.-T. Liu, X.-M. Shi, X.-Y. Lang, L. Gu, Z. Wen, M. Zhao and Q. Jiang, *Nat. Commun.*, 2018, **9**, 1375.

9 P. Simon and Y. Gogotsi, *Nat. Mater.*, 2008, **7**, 845–854.

10 M. R. Lukatskaya, O. Mashtalir, C. E. Ren, Y. Dall'Agnese, P. Rozier, P. L. Taberna, M. Naguib, P. Simon, M. W. Barsoum and Y. Gogotsi, *Science (80-.).*, 2013, **341**, 1502–1505.

11 P. Simon and Y. Gogotsi, *Nat. Mater.*, 2008, **7**, 845–854.

12 M. Acerce, D. Voiry and M. Chhowalla, *Nat. Nanotechnol.*, 2015, **10**, 313–318.

13 Y. Xu, Y. Tao, X. Zheng, H. Ma, J. Luo, F. Kang and Q. Yang, *Adv. Mater.*, 2015, **27**, 8082–8087.

14 J. Kang, A. Hirata, L. Chen, S. Zhu, T. Fujita and M. Chen, *Angew. Chemie Int. Ed.*, 2015, **54**, 8100–8104.

15 X. Tang, R. Jia, T. Zhai and H. Xia, *ACS Appl. Mater. Interfaces*, 2015, **7**, 27518–27525.

16 S. Lin, C. Zhang, Z. Wang, S. Dai and X. Jin, *Adv. Energy Mater.*, 2017, **7**, 1700766.

17 G. Lian, C.-C. Tuan, L. Li, S. Jiao, K.-S. Moon, Q. Wang, D. Cui and C.-P. Wong, *Nano Lett.*, 2017, **17**, 1365–1370.

18 Z. Fan, Z. Cheng, J. Feng, Z. Xie, Y. Liu and Y. Wang, *J. Mater. Chem. A*, 2017, **5**, 16689–16701.

19 M. R. Lukatskaya, S. Kota, Z. Lin, M.-Q. Zhao, N. Shpigel, M. D. Levi, J. Halim, P.-L. Taberna, M. W. Barsoum, P. Simon and Y. Gogotsi, *Nat. Energy*, 2017, **2**, 17105.

20 H. Ma, D. Kong, Y. Xu, X. Xie, Y. Tao, Z. Xiao, W. Lv, H. D. Jang, J. Huang and Q. Yang, *Small*, 2017, **13**, 1701026.

21 P. Wu, S. Cheng, M. Yao, L. Yang, Y. Zhu, P. Liu, O. Xing, J. Zhou, M. Wang, H. Luo and M. Liu, *Adv. Funct. Mater.*, 2017, **27**, 1702160.

22 S. Kalasina, N. Phattharasupakun and M. Sawangphruk, *J. Mater. Chem. A*, 2018, **6**, 36–40.

23 L. Qin, Q. Tao, A. El Ghazaly, J. Fernandez-Rodriguez, P. O. Å. Persson, J. Rosen and F. Zhang, *Adv. Funct. Mater.*, 2018, **28**, 1703808.

24 H. Jeon, J. Jeong, H. G. Kang, H.-J. Kim, J. Park, D. H. Kim, Y. M. Jung, S. Y. Hwang, Y. Han and B. G. Choi, *Adv. Energy Mater.*, 2018, **8**, 1800227.

25 E. Kayali, A. VahidMohammadi, J. Orangi and M. Beidaghi, *ACS Appl. Mater. Interfaces*, 2018, **10**, 25949–25954.

26 A. VahidMohammadi, J. Moncada, H. Chen, E. Kayali, J. Orangi, C. A. Carrero and M. Beidaghi, *J. Mater. Chem. A*, 2018, **6**, 22123–22133.

27 A. VahidMohammadi, M. Mojtabavi, N. M. Caffrey, M. Wanunu and M. Beidaghi, *Adv. Mater.*, 2019, **31**, 1806931.

28 T. Gao, Z. Zhou, J. Yu, J. Zhao, G. Wang, D. Cao, B. Ding and Y. Li, *Adv. Energy Mater.*, 2019, **9**, 1802578.

29 Y. Dong, S. Zhang, X. Du, S. Hong, S. Zhao, Y. Chen, X. Chen and H. Song, *Adv. Funct. Mater.*, 2019, **29**, 1901127.

30 S. S. Mofarah, E. Adabifiroozjaei, Y. Yao, P. Koshy, S. Lim, R. Webster, X. Liu, R. Khayyam Nekouei, C. Cazorla, Z. Liu, Y. Wang, N. Lambropoulos and C. C. Sorrell, *Nat. Commun.*, 2019, **10**, 2594.

31 K. Li, X. Wang, X. Wang, M. Liang, V. Nicolosi, Y. Xu and Y. Gogotsi, *Nano Energy*, 2020, **75**, 104971.

32 G. Wu, T. Li, Z. Wang, M. Li, B. Wang and A. Dong, *Angew. Chemie Int. Ed.*, 2020, **59**, 20628–20635.